Modeling of borophene with density-functional tight-binding

Master's thesis, March 18, 2020

Author:

Eerik ukkola

Supervisor:

Pekka Koskinen

JYVÄSKYLÄN YLIOPISTO
FYSIIKAN LAITOS

Abstract

Ukkola, Eerik
Modeling of borophene with density-functional tight-binding
Master's thesis
Department of Physics, University of Jyväskylä, 2020, 43 pages.

Borophene is a recently discovered two-dimensional allotrope of boron that has shown unique electromechanical properties. In this study mechanical properties of borophene are modeled with density-functional tight-binding (DFTB), which is a method derived from density-functional theory (DFT). The goal of the study is to obtain direction-dependent bending stiffness of borophene by utilizing revised periodic boundary conditions (RPBC). The bending process can be simulated by applying RPBC and creating copies of the initial borophene unit cell that are translated and rotated. Difficulties arose during parametrization process of DFTB, since not all mechanical constants matched with DFT results. The DFTB results were exotic and indicated that one type of borophene lattice has negative bending stiffness. DFT calculations were conflicting and showed that DFTB calculations are likely to be inaccurate. Ultimately it was concluded that DFTB may not be a reliable method for modeling borophene.

Keywords: borophene, DFTB, bending, DFT, electronic structure analysis, 2D materials, RPBC

Tiivistelmä

Ukkola, Eerik
Borofeenin mallintaminen tiheysfunktionaaliteoriaan perustuvalla tiukan sidonnan mallilla
Pro gradu -tutkielma
Fysiikan laitos, Jyväskylän yliopisto, 2020, 43 sivua

Borofeeni on äskettäin löydetty boorin kaksiulotteinen allotrooppi. Materiaalilla on ainutlaatuisia elektromekaanisia ominaisuuksia, mikä tekee siitä kiinnostavan useiden eri sovellusten kannalta. Tässä tutkimuksessa borofeenia mallinnetaan tiheysfunktionaaliteoriaan perustuvalla tiukan sidonnan mallilla (DFTB). Tutkimuksen tavoitteena oli laskea borofeenin suunnasta riippuva taivutusmoduuli hyödyntämällä mukautettuja periodisia reunaehtoja (RPBC). Taivutusprosessia simuloidaan luomalla alkupäisestä borofeenin yksikkökopista kopioita, jotka sopivasti aseteltuna tekevät rakenteesta efektiivisesti taivutetun. DFTB:n parametrisoinnissa tuli kuitenkin ongelmia, kun osa borofeenin mekaanisista vakioista ei vastannutkaan DFT:llä laskettuja referenssiarvoja. Lopulliset DFTB:llä saadut tulokset olivat erikoisia, sillä erään borofeenihilan taivutusmoduuli oli negatiivinen. Saatuja tuloksia vertailtiin DFT-tulosten kanssa, ja vaikuttaa siltä, että DFTB ei ole kaikissa tilanteissa luotettava metodi borofeenin mallintamissa.

Avainsanat: borofeeni, DFTB, taivutus, DFT, elektronirakenneanalyysi, 2D materiaalit, RPBC

Contents

1 Introduction

Since discovery of graphene in 2004 [1], two-dimensional (2D) materials have attracted plenty of attention. There are many existing 2D allotropes such as graphene, borophene, germanene, phosphorene and silicene, and even a greater number of compound materials. There are also a lot of 2D materials that have been theoretically predicted but have not been successfully synthesized yet. [2]

What makes 2D materials interesting is their unique properties compared to regular 3D materials. High surface-to-volume ratio enhances their capabilities for energy storage and catalysis, and lack of dangling bonds can make them effective semiconductors through increased charge carrier mobility [3]. Due to these properties, typical applications for 2D materials are semiconductors and photovoltaics, although new places for applications are constantly searched for.

Graphene is by far the most researched 2D material, since it has proven itself useful in commercial applications and is relatively easy to synthesize. However breakthrough of graphene raises the question whether other potent new materials can be found, which makes researching and exploring new materials important. This study will focus on one of the recently synthesized 2D materials, borophene.

Borophene (Figure 1) is a two-dimensional allotrope of boron, which is a metalloid with atomic number 5. The low number of valence electrons has interesting consequences and gives borophene unique physical and chemical properties as a two-dimensional material. Unlike typical two-dimensional structures, borophene does not have a single well-defined crystal structure - instead its structure depends on the metal substrate it is grown on. Due to interactions between formed borophene layer and substrate, moving free-standing borophene on other surfaces is a challenge since the stability of the lattice is affected by the substrate [4].

Borophene sheets can be thought of consisting of triangular lattice with hexagonal vacancies. The tendency to have vacancies in the boron lattice is due to boron's electron structure. For completely hexagonal lattice (like graphene's), there are not enough electrons to fill all stabilizing sp^2 and p_z bonding states, which makes that configuration unfavourable [5]. On the other hand flat triangular would have

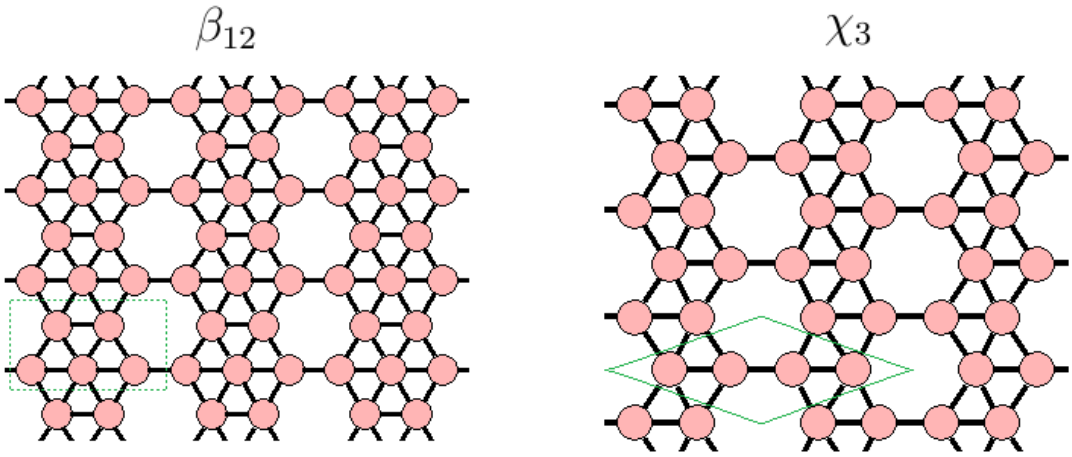

Figure 1. β_{12} and χ_3 borophene lattices. β_{12} has vacancy concentration of 1/6 and for χ_3 $v = 1/5$. Unit cells are marked with green.

two electrons on high-energy antibonding states, and thus triangular borophene breaks the symmetry instead and favours buckled conformation [5]. Flat and the most stable borophene sheets alter between two-center and three-center bonding, since then all in-plane bonding states become filled while antibonding states remain empty [5]. From figure 2 it can be seen that total energy per boron atom has a minimum at vacancy concentration $v = 1/9$, leading to most stable borophene structure. The minimum is relatively broad: borophene sheets $v = 1/6$ and $v = 1/12$ are approximately 10 meV/atom above the minimum as can be seen in figure 2. As vacancy concentrations grow larger the energy starts to increase quickly and structures turn less stable (Figure 2), and thus borophene cannot form graphene-like structures. While other borophene lattices are planar, triangular borophene lattice with no vacancies actually consist of two square lattices located at different levels. A study by Zhang et al. [4] predicts triangular lattice to have high energy in vacuum but be more stable on metal substrates. This study will focus more closely on two borophene lattices, β_{12} ($v = 1/6$) and χ_3 ($v = 1/5$), both presented in figure 1. These lattices are among the most stable borophene crystal structures.

There are multiple potential applications for borophene. A few of them are briefly discussed here, starting from hydrogen storage. Hydrogen has excellent energy density by weight, and is therefore a great candidate as an energy source for example for vehicles. However storing hydrogen efficiently is difficult, since as a gas it has low density and requires large stores and as a liquid it has to be heavily compressed.

This is where borophene may prove itself helpful. While binding energy of hydrogen to plain borophene is too low (~0.05 eV) for practical storaging, borophene decorated with alkali metals (Figure 3) is efficient at adsorbing hydrogen molecules [6], with binding energy up to 0.35 eV and weight percent capacity of 6.8-15.26 wt % for different lattice types with lithium. In comparison, storage capacity of MoS_2 is 4.8 wt % [7] and for silecene 6.35 wt % [8]. Graphene, on the other hand, has high weight capacity 12.8 wt % [9], but in graphene alkali metals tend to form clusters, making it a difficult substrate [6].

Another energy source related potential application is high power density batteries [10]. Current rechargable lithium-ion batteries have relatively high power capacity and life-time, but their capacity is still insufficient for power-intensive purposes, since the required battery sizes would have to be impractically large. Borophene and other 2D materials are promising candidates for electrodes, which have a crucial role in battery performance [10]. Zhang et al. showed in their study [10] that β_{12} borophene can have theoretical storage capacity of 1984 mAh/g, which greatly surpasses that of commercial graphite (372 mAh/g), phosphorene (433 mAh/g) and silicene (954 mAh/g). High conductance of borophene also makes it suitable for fast charging and discharging. [11]

Since borophene has been successfully synthesized recently for the first time (2015 [12]), it has not been extensively studied. Mechanical properties of borophene have been studied previously by for example Singh et al. [13] and Zhang et al. [14]. This study aims to extend their research by calculating direction-dependent bending stiffness of borophene, while they have computed it only for principal lattice directions. The method chosen is density-functional tight-binding, which is a computationally lighter method than the more commonly used density-functional theory.

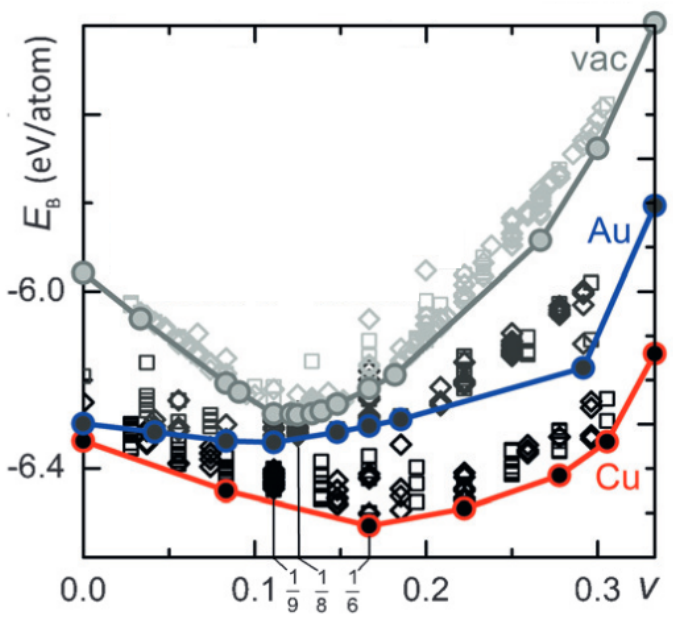

Figure 2. Binding energy per atom in different borophene lattices and substrates. Adapted with permission from Zhang et al. [4], edited. Copyright 2015 Angewandte Chemie International Edition.

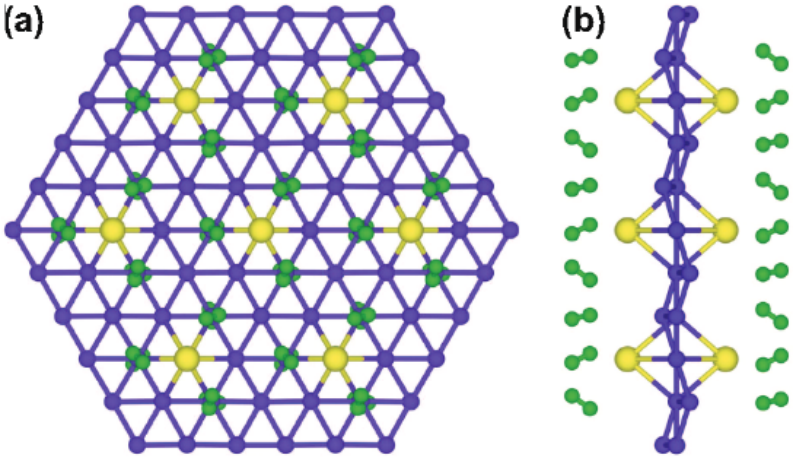

Figure 3. Illustration of how hydrogen molecules are adsorbed around alkali metals on borophene sheet. Reprinted (adapted) with permission from Er et al. [6]. Copyright 2009 American Chemical Society.

2 Theoretical background

Properties of two-dimensional materials are dominated by quantum level effects, mainly by their electronic structure. Thus modeling their mechanical properties requires electron structure analysis. There are many methods for this, each of which has their area where they are applicable. One of the most used methods for simulating atom systems is density functional theory (DFT), but it comes with the drawback of being computationally expensive, which tends to make it ineffective for large systems. An alternative method for analysis is density functional tight binding (DFTB), which is an approximation based on DFT.

As DFT is a quantum computational method, it essentially tries to find a solution to the many-body problem. Foundations of DFT were created in 1964 when Hohenberg and Kohn showed in their paper that electron density n can be used to determine properties of an N-electron system exactly [15]. According to their work, there's unique potential $\vec{V}_{\text{ext}}$ for each electron density n_x, and correspondingly unique ground state wave function Ψ_0. In 1965 Kohn and Sham extended the work [16] and made density functional theory more applicable by approximating interacting electrons system by non-interacting electron system. In the approximation kinetic energy $T_s[n]$ and classical electrostatic energy E_H have simple forms, since the particles are non-interacting. Third term, exchange-correlation energy E_{xc}, contains remaining differences in energy between the fictious non-interacting system and the true interacting system. Thus the true system can be treated as a non-interacting system in an effective potential V_{KS}, which has the same ground state density n as the interacting system.

DFT is computationally expensive method, which makes simulating large systems with it slow. A faster method, density-functional tight-binding (DFTB), can be derived from Kohn-Sham DFT by making further approximations. By approximating that electrons are localized at atomic sites electronic wave functions can be presented as a linear combination of atomic orbitals, which is easy basis to use in practice. [17].

This section starts by briefly reviewing DFT. Next DFTB is derived from DFT and the main approximations of DFTB are shown. Finally revised boundary conditions

(RPBC) are considered, since they are crucial for modeling bending of the atom layers. All equations are presented in atomic units.

2.1 Density-functional theory

The origin of DFT, like other quantum computational methods, is in many-body problem. Schrödinger equation for a system of electrons in an external potential is

$$\hat{H}\Psi\left(\vec{r}_1,\vec{r}_2,...\right)=\hat{H}\Psi\left(\vec{r}\right)=\left[\hat{T}+\hat{V}_{\text{ext}}+\hat{U}_{\text{e}}\right]\Psi\left(\vec{r}\right) \tag{1}$$

$$=\left[-\frac{1}{2}\sum_I\nabla_I^2+\frac{1}{2}\sum_{J\neq I}\sum_I\frac{1}{|\vec{r_I}-\vec{r_J}|}+\sum_I V_{\text{ext}}\left(r_I\right)\right]\Psi\left(\vec{r}\right)=E\Psi\left(\vec{r}\right), \tag{2}$$

where $\hat{T}$ is kinetic energy operator, $\hat{V}_{\text{ext}}$ external potential from nuclei and $\hat{U}_{\text{e}}$ potential electrons express on each other.

By defining the electronic part of the Hamiltonian as

$$\hat{F}=-\frac{1}{2}\sum_I\nabla_I^2+\frac{1}{2}\sum_{J\neq I}\sum_I\frac{1}{|\vec{r_I}|} \tag{3}$$

the total Hamiltonian can be written as

$$\hat{H}=\hat{F}+\hat{V}_{\text{ext}}. \tag{4}$$

Hohenberg and Kohn showed in their paper in 1964 [18] that the external potential $\hat{V}_{\text{ext}}$ is also uniquely determined by the corresponding ground state density $n\left(\vec{r}\right)$. The proof is simple. If $\hat{V}_{\text{ext}}$ is not uniquely determined by $n\left(\vec{r}\right)$, there must exist another external potential $\hat{V}'_{\text{ext}}$ with ground state $\Psi'\left(\vec{r}\right)$ that has corresponding ground state density $n\left(\vec{r}\right)$. Hamiltonian $\hat{H}'=\hat{F}+V'_{\text{ext}}$ for such system and its ground state energy $E'=\langle\Psi'|\,\hat{H}\,|\Psi'\rangle$.

Since wave functions $\Psi\left(\vec{r}\right)$ and $\Psi'\left(\vec{r}\right)$ cannot be the same, $\Psi'\left(\vec{r}\right)$ cannot be a ground state of $\hat{H}$ and following inequalities must apply:

$$\langle\Psi|\,\hat{H}\,|\Psi\rangle=E<\langle\Psi'|\,\hat{H}\,|\Psi'\rangle \tag{5}$$

$$\langle\Psi'|\,\hat{H}'\,|\Psi'\rangle=E'<\langle\Psi'|\,\hat{H}\,|\Psi'\rangle\,. \tag{6}$$

Opening the right sides of inequalities (5) and (6) leads to expressions

$$\begin{aligned}\langle\Psi'|\,\hat{H}\,|\Psi'\rangle &= \langle\Psi'|\,\hat{H}'\,|\Psi'\rangle + \langle\Psi'|\left(\hat{H}'-\hat{H}\right)|\Psi'_0\rangle \\ &= E' + \int n\left(\vec{r}\right)\left(V_{\text{ext}}\left(\vec{r}\right) - V'_{\text{ext}}\left(\vec{r}\right)\right)d^3r\end{aligned} \tag{7}$$

and

$$\begin{aligned}\langle\Psi|\,\hat{H}'\,|\Psi\rangle &= \langle\Psi|\,\hat{H}\,|\Psi\rangle + \langle\Psi|\left(\hat{H}-\hat{H}'\right)|\Psi\rangle \\ &= E - \int n\left(\vec{r}\right)\left(V_{\text{ext}}\left(\vec{r}\right) - V'_{\text{ext}}\left(\vec{r}\right)\right)d^3r.\end{aligned} \tag{8}$$

Combining inequalities (5) and (6) with expressions (7) and (8) lead to conclusion that $E + E' < E + E'$, which by contradiction proofs that ground state density $n\left(\vec{r}\right)$ uniquely determines the external potential V_{ext}.

Since ground state density n has a corresponding ground state Ψ with energy $E = E_0$, the ground state can be found by minimizing functional

$$E\left[n\left(\vec{r}\right)\right] = F\left[n\left(\vec{r}\right)\right] + \int V_{\text{ext}}\left(\vec{r}\right)n\left(\vec{r}\right)dr, \tag{9}$$

where functional $F\left[n\left(\vec{r}\right)\right]$ is defined as

$$F\left[n\left(\vec{r}\right)\right] = \langle\Psi|\left(\hat{T}+\hat{U}_e\right)|\Psi\rangle\,. \tag{10}$$

Kohn and Sham introduced a method to rewrite the problem of interacting electrons as a problem of fictious non-interacting electrons. This allows reducing the wave function to three dimensions, rather that 3N-dimensions. First, functional $F\left[n\right]$ is split into three terms:

$$F\left[n\right] = T_s\left[n\right] + \frac{1}{2}\int\int\frac{n\left(\vec{r}\right)n\left(\vec{r}'\right)}{|\vec{r}-\vec{r}'|}d^3r\,d^3r' + E_{\text{xc}}\left[n\right], \tag{11}$$

where $T_s\left[n\right]$ is kinetic energy of non-interacting electrons and $E_{\text{xc}}\left[n\right]$ is the error term known as exchange-correlation energy.

The term

$$E_{\text{H}}\left[n\left(\vec{r}\right)\right] = \frac{1}{2}\int\int\frac{n\left(\vec{r}\right)n\left(\vec{r}'\right)d^3r\,d^3r'}{|\vec{r}-\vec{r}'|} \tag{12}$$

is known as Hartree energy E_{H}. By definition exchange-correlation energy can then be written as

$$E_{\text{xc}} = \left(T - T_{\text{s}}\right) + \left(E_{\text{ee}} - E_{\text{H}}\right), \tag{13}$$

where E_{ee} is potential energy of the interacting electron system.

Using Lagrange multiplier method to limit the number of electrons as N for density-functional (9) the variational problem can be written as

$$\delta\left[F\left[n\left(\vec{r}\right)\right]\right]+\int V_{\mathrm{ext}}\left(\vec{r}\right)n\left(\vec{r}\right)d^{3}r-\mu\left(\int n\left(\vec{r}\right)d^{3}r-N\right)=0. \tag{14}$$

By defining Kohn-Sham potential $V_{\mathrm{KS}}\left(\vec{r}\right)$ as

$$V_{\mathrm{KS}}\left(\vec{r}\right)=\int\frac{n\left(\vec{r}'\right)}{\left|\vec{r}-\vec{r}'\right|}d^{3}r'+V_{\mathrm{xc}}\left(\vec{r}\right)+V_{\mathrm{ext}}\left(\vec{r}\right), \tag{15}$$

where exchange-correlation potential $V_{\mathrm{xc}}\left(\vec{r}\right)$ is

$$V_{\mathrm{xc}}\left(\vec{r}\right)=\frac{\delta E_{\mathrm{xc}}\left[n\right]}{\delta n\left(\vec{r}\right)}, \tag{16}$$

the variational problem (14) can be written in the form

$$\frac{\delta T_{s}\left[n\right]}{\delta n\left(\vec{r}\right)}+V_{\mathrm{KS}}\left(\vec{r}\right)=\mu. \tag{17}$$

Equation (17) is the same equation as what would be obtained for non-interacting particles moving in an external potential $V_{\mathrm{KS}}\left(\vec{r}\right)$. Thus the initial problem of interacting particles is mapped into a problem on non-interacting particles. One-electron Schrödinger equations for this system are then

$$\left[-\frac{1}{2}\nabla^{2}+V_{\mathrm{KS}}\left(\vec{r}\right)\right]\psi_{a}\left(\vec{r}\right)=\epsilon_{a}\psi_{a}\left(\vec{r}\right), \tag{18}$$

where $\psi_{a}\left(\vec{r}\right)$ are single-particle states with energies ϵ_{a}.

Electron density is then

$$n\left(\vec{r}\right)=\sum_{a}f_{a}|\psi_{a}\left(\vec{r}\right)|^{2}, \tag{19}$$

where f_{a} is occupation of single-particle state ψ_{a}, belonging into range $[0,2]$ since electrons are fermions.

Non-interacting kinetic energy is

$$T_{s}\left[n\right]=-\sum_{a}\frac{f_{a}}{2}\int\psi_{a}^{*}\left(\vec{r}\right)\nabla^{2}\psi_{a}\left(\vec{r}\right)d^{3}r. \tag{20}$$

Using equations (12) and (15) the total energy of the system is

$$E\left[n\left(\vec{r}\right)\right]=T_{\mathrm{s}}\left[n\left(\vec{r}\right)\right]+\int V_{\mathrm{ext}}\left(\vec{r}\right)n\left(\vec{r}\right)d^{3}r+\frac{1}{2}\int\int\frac{n\left(\vec{r}\right)n\left(\vec{r}'\right)d^{3}r\,d^{3}r'}{\left|\vec{r}-\vec{r}'\right|}+E_{xc}\left[n\right]. \tag{21}$$

2.2 From density-functional theory to density-functional tight-binding

Density-functional tight-binding is an approximation derived from DFT. Tight-binding is based on the assumption that electrons are localized at atomic sites and can thus be presented as superposition of localized wave functions.

The main points of the derivation for expression of energy in DFTB are shown here. Derivation mostly follows article by Koskinen and Mäkinen [19]. The starting point for DFTB energy is Kohn-Sham energy (21). In sum form Kohn-Sham energy (21) is

$$E\left[n\right]=\sum_{a}f_{a}\left\langle\psi_{a}\right|\left(-\frac{1}{2}\nabla^{2}+\int V_{\mathrm{ext}}\left(\vec{r}\right)n\left(\vec{r}\right)+\frac{1}{2}\int\frac{n(r')d^{3}r'}{\left|r'-r\right|}\right)\left|\psi_{a}\right\rangle+E_{\mathrm{xc}}. \tag{22}$$

Equation (22) is the accurate energy of the system, since exchange-correlation energy E_{xc} contains all quantum many-body effects. Energy in DFTB is derived from equation (22) with second order expansion respect to density $n(\vec{r})$. The expansion is based on the assumption that density $n(\vec{r})$ deviates only slightly from the density of free and neutral atoms and can thus be approximated as

$$n(r)=n_{0}(\vec{r})+\delta n_{0}(\vec{r}), \tag{23}$$

where $n_0(r)$ is the density of free and neutral atoms and $\delta n_0(r)$ a small fluctuation. A second order expansion of $E\left[n\right]$ is then [19]

$$\begin{aligned}E\left[\delta n\right]\approx&\sum_{a}f_{a}\left\langle\psi_{a}\right|-\frac{1}{2}\nabla^{2}+V_{\mathrm{ext}}+V_{\mathrm{H}}\left[n_{0}\right]+V_{\mathrm{xc}}\left[n_{0}\right]\left|\psi_{a}\right\rangle\\&+\frac{1}{2}\int\int\left(\frac{\delta^{2}E_{\mathrm{xc}}\left[n_{0}\right]}{\delta n\delta n'}+\frac{1}{\left|r-r'\right|}\right)\delta n\delta n'd^{3}rd^{3}r'\\&-\frac{1}{2}\int V_{\mathrm{H}}\left[n_{0}\right]\left(r\right)n_{0}\left(r\right)d^{3}r+E_{\mathrm{xc}}\left[n_{0}\right]-\int V_{\mathrm{xc}}\left[n_{0}\right]\left(r\right)n_{0}\left(r\right)d^{3}r.\end{aligned} \tag{24}$$

Equation 24 consists of multiple terms that are viewed separately. The first of them is band structure energy E_{BS}:

$$E_{BS}\left[\delta n\right]=\sum_{a}f_{a}\left\langle\psi_{a}\right|H\left[n_{0}\right]\left|\psi_{a}\right\rangle. \tag{25}$$

Second term describes Coulomb energy with a contribution from exchange-correlation energy

$$E_{\mathrm{coul}}\left[\delta n\right]=\frac{1}{2}\int\int\left(\frac{\delta^{2}E_{\mathrm{xc}}\left[n_{0}\right]}{\delta n\delta n'}+\frac{1}{\left|r-r'\right|}\right)\delta n\delta n'd^{3}rd^{3}r'. \tag{26}$$

Finally what is left is so called repulsive energy, which consists of four terms

$$E_{\text{rep}} = -\frac{1}{2}\int\int \frac{n_0\left(\vec{r}\right) n_0\left(\vec{r'}\right) d^3r\, d^3r'}{\left|\vec{r}-\vec{r'}\right|} + E_{\text{xc}}\left[n_0\right] - \int V_{\text{xc}}\left[n_0\right]\left(\vec{r}\right) n_0\left(\vec{r}\right) d^3r. \quad (27)$$

Repulsive energy term is also considered more closely for further approximations. The first term in equation (27), Hartree energy term, is a double integral over electron densities. When the integration space is divided into atomic volumes ν_I, total contribution to charge from density n_0 confined in the volume is practically just the number of electrons of a free atom. The exact form of the xc-terms is unknown, but they depend on spherically symmetric electron density and can be approximated as a repulsive function depending on atomic distances R_{IJ}. The approach for the repulsive potential in DFTB is semi-experimental and it is obtained from a fitting process. The whole repulsive energy term can then be approximated as [19]

$$E_{rep} = \sum_{I<J} V_{\text{rep}}^{IJ}\left(R_{IJ}\right), \quad (28)$$

where V_{rep}^{IJ} is the repulsive potential. The data used for fitting can for example be from experiments or DFT-calculations. This fitting process is described in more detail in section 3.

The next term to be discussed is Coulomb energy (26). The term consists a double integral that has to be converted into a sum so that it can be evaluated. This is again achieved by dividing integration space into volumes ν_I corresponding to atoms I [19]. An integral over volume ν_I is then approximately the charge fluctuation of atom I

$$\Delta q_I \approx \int_{\nu_I} \delta n\left(\vec{r}\right) d^3r \quad (29)$$

and density fluctuation

$$\delta n\left(\vec{r}\right) = \sum_I \Delta q_I \delta n_I\left(\vec{r}\right), \quad (30)$$

where density contribution δn_I from atom I is normalized so that

$$\int_{\nu_I} \delta n_I\left(\vec{r}\right) d^3r = 1. \quad (31)$$

Since Coulomb energy (26) includes xc-contributions that are complicated, the approach in DFTB is approximating them with more simple functions. For this

purpose an approximation for atom energy from quantum chemistry is useful. Atom energy as a function of charge fluctuation Δq can be approximated as [19]

$$\begin{aligned} E\left(\Delta q\right) \approx & E_0 + \left(\frac{\partial E}{\partial \Delta q}\right)\Delta q + \frac{1}{2}\left(\frac{\partial^2 E}{\partial \Delta q^2}\right)\Delta q^2 \\ = & E_0 - \chi \Delta q + \frac{1}{2} U \Delta q^2, \end{aligned} \tag{32}$$

where χ is electronegativity and U is Hubbard U.

Approximate expressions for electronegativity and Hubbard U are

$$\chi \approx \frac{1}{2}\left(IE + EA\right) \tag{33}$$

$$U \approx IE - EA, \tag{34}$$

where IE is ionization energy and EA is electron affinity.

Now, Coulomb energy (26) can be divided into sums over all atom pairs IJ. There are two kind of terms in the sum for Coulombic interaction between atoms I and J. In the first case $I = J$, and the term becomes

$$E_{I=J} = \frac{1}{2}\Delta q_I^2 \int_{\nu_I}\int_{\nu_I}\left(\frac{\delta^2 E_{\mathrm{xc}}\left[n_0\right]}{\delta n \delta n'} + \frac{1}{|\vec{r} - \vec{r'}|}\right)\delta n_I \delta n_I' d^3 r d^3 r'. \tag{35}$$

By using Hubbard U from equation (32), expression (35) can be approximated as

$$E_{I=J} \approx \frac{1}{2} U_I \Delta q_I^2. \tag{36}$$

In the second case $I \neq J$, but that means xc-contributions vanish in the limit of interatomic distances, and what is left of the term is

$$E_{I\neq J} = \frac{1}{2}\Delta q_I \Delta q_J \int_{\nu_I}\int_{\nu_I}\frac{1}{|\vec{r} - \vec{r'}|}\delta n_I \delta n_J' d^3 r d^3 r'. \tag{37}$$

This is still not enough to explicitly evaluate the term, since functions $\delta n_I(\vec{r})$ are not defined. At this point they are assumed to be spherically symmetric Gaussian distributions:

$$\delta n_I(\vec{r}) = \frac{1}{\left(2\pi\sigma_I^2\right)^{\frac{3}{2}}}\exp\left(-\frac{r^2}{2\sigma_I^2}\right), \tag{38}$$

where standard deviation σ_I is obtained from full width at half maximum of the Gaussian distribution:

$$\sigma_I = \frac{\mathrm{FWHM}_I}{\sqrt{8\ln 2}}. \tag{39}$$

Using of Gaussian distribution is argued by Koskinen and Mäkinen in their article [19]. Gaussian distributions are highly localized, and thus integrating over volume ν_I surrounding the distribution is a valid approximation for integrating over the whole space.

Thus expression for $I \neq J$ terms becomes

$$\int_{\nu_I}\int_{\nu_J} \frac{\delta n_I \delta n'}{|\vec{r} - \vec{r'}|} = \frac{\operatorname{erf}(C_{IJ} R_{IJ})}{R_{IJ}} \equiv \gamma_{IJ}(R_{IJ}), \tag{40}$$

where C_{IJ} is defined as

$$C_{IJ} = \sqrt{\frac{4 \ln 2}{\mathrm{FWHM}_I^2 + \mathrm{FWHM}_J^2}}. \tag{41}$$

At the limit $R \to 0$, $\gamma \to C \cdot 2/\sqrt{\pi}$, which yields expression for FWHM:

$$\mathrm{FWHM}_I = \sqrt{\frac{8 \ln 2}{\pi} \frac{1}{\mathrm{U}_I}}. \tag{42}$$

Finally the coulombic energy term can be presented as

$$E_{\mathrm{coul}} = \frac{1}{2} \sum_I \sum_J \gamma_{IJ}(R_{IJ}) \Delta q_I \Delta q_J, \tag{43}$$

where γ_{IJ} depends on indices as

$$\gamma_{IJ}(R_{IJ}) = \begin{cases} \mathrm{U}_I, & \text{if } I = J \quad (44) \\ \dfrac{\operatorname{erf}(C_{IJ} R_{IJ})}{R_{IJ}}, & \text{if } I \neq J. \quad (45) \end{cases}$$

So far from introduced variables U and the related FWHM are parameters. Hubbard U can be derived from equation (34) and it is found from standard tables. The next section will introduce more essential parameters for DFTB, and how parameters are adjusted is considered in section 3.

2.3 Tight-binding and pseudo-atoms

Next basis functions are considered more closely. Since tight-binding assumes that electrons are located at atomic sites, single-electron wave functions $\psi_a(\vec{r})$ can be presented in form

$$\psi_a(\vec{r}) = \sum_\mu c_\mu^a \varphi_\mu(\vec{r}), \tag{46}$$

where c_μ^a are coefficients and φ_μ localized basis functions.

A natural choice for minimal local basis is spherical functions

$$\varphi_\mu(\vec{r}) = R_\mu(\vec{r})\, Y_\mu(\theta, \varphi), \tag{47}$$

where Y_μ are (real) spherical harmonics. However since electrons are assumed to be tighly bound, orbitals of free electrons are not sufficient, as they extend to infinity. Thus the used orbitals are from pseudo-atoms, which are created by adding an artificial confinement potential, which damps the tails of the orbitals. The Hamiltonian for a pseudo-atom is then [19]

$$H_p = -\frac{1}{2}\nabla^2 - \frac{Z}{r} + V_{\mathrm{H}} + V_{\mathrm{xc}} + V_{\mathrm{conf}}, \tag{48}$$

where V_{conf} is a damping potential that cuts the orbital after a certain range. Since odd terms have to vanish at $V_{\mathrm{conf}}(\vec{r} = 0)$, lowest-order approximation for damping potential is

$$V_{\mathrm{conf}} = \left(\frac{\vec{r}}{r_0}\right)^2, \tag{49}$$

where r_0 is a parameter determining strength of the confinement potential. Adjusting r_0 is discussed more closely in section 3.

The orbitals $\varphi_\mu(\vec{r})$ are computed once for each element pair (each confinement potential) with LDA-DFT during parametrization [19] and are stored in tables.

Next eigenstates $|\psi_a\rangle$ and populations Δq_I are considered through tight-binding approach. Tight-binding is based on the assumption that electrons are localized at atomic sites and can thus be presented as superposition of localized wave functions.

By substituting equation (46) into expression of band-structure energy (25), it becomes

$$E_{\mathrm{BS}} = \sum_a f_a \sum_\mu \sum_\nu c_\mu^{a*} c_\nu^a H_{\mu\nu}^0, \tag{50}$$

where matrix element $H_{\mu\nu}^0$ is defined as

$$H_{\mu\nu}^0 = \langle \varphi_\mu | H^0 | \varphi_\nu \rangle. \tag{51}$$

How integral (51) is evaluated will be discussed below after introducing overlap integrals.

Charge fluctuations Δq still have to be defined to be able to calculate total energy. This can be obtained from total number of electrons by the evaluating amount of charge within volume ν_I of atom I. Total number of electrons of atom I is then

$$q_I = \sum_a f_a \int_{\nu_I} |\psi_a|^2 d^3r = \sum_a f_a \sum_\mu \sum_\nu c_\mu^{a*} c_v^a \int_{\nu_I} \varphi_\mu^* \varphi_v d^3r. \tag{52}$$

The last integral in equation (52) is familiar from chemistry and it is known as the orbital overlap integral $S_{\mu\nu} = \langle \varphi_\mu | \varphi_\nu \rangle$. The integral $S_{\mu\nu}$ has three cases. If orbitals μ and ν belong to atom I, the integral is $\delta_{\mu\nu}$ due to orthonormality of the orbitals. If neither of the orbitals belong to atom I, the integral is approximately zero. The last case is non-trivial. In the case that one of the orbitals belongs to atom I and the other orbital belongs to another atom J, the integral is approximately half of orbital overlap integral $S_{\mu\nu}$, since half of the overlap occurs within volume v_I. [19]

Since the basis functions were defined as real spherical harmonics, orbital overlap integral

$$S_{\mu\nu} = \int \varphi_\mu^* (\vec{r}) \, \varphi_\nu (\vec{r}) \, d^3 r \tag{53}$$

can be calculated with their distance vector $\vec{R}_{IJ}$ as the variable. Following from the properties of spherical harmonics, Slater-Koster transformation rules apply to $\vec{R}_{IJ}$ dependence. Thus $S_{\mu\nu}$ for each orbital pair can be calculated at enough dense set of R_{IJ} and stored in tables, from which the overlap can be computed quickly later. Since matrix elements $H^0_{\mu\nu}$ also obey Slater-Koster transformation rules, they can be evaluated similarly. [20]

With overlap integrals defined, total number of electrons within volume v_I is then

$$q_I = \sum_a f_a \sum_{\mu \in I} \sum_\nu \left(c_\mu^{a*} c_v^a + c_\mu^a c_v^{a*} \right) S_{\mu\nu}. \tag{54}$$

Charge fluctuation Δq_I is then obtained from total number of electrons q_I by reducing the number of valence electrons q_I^0 in neutral atom from it.

Since all variables are defined, with expressions (28), (43) and (54) combined the total energy is

$$E = \sum_a f_a \sum_\mu \sum_\nu c_\mu^{a*} c_\nu^a H^0_{\mu\nu} + \frac{1}{2} \sum_I \sum_J \gamma_{IJ} (R_{IJ}) \, \Delta q_I \Delta q_J + \sum_{I<J} V_{\text{rep}}^{IJ} (R_{IJ}) \, . \tag{55}$$

In practice $H^0_{\mu\nu}$, γ_{IJ} and V_{rep}^{IJ} are all related to parameters that are set during parametrization. This process is described in section 3.

2.4 Revised periodic boundary conditions

Crystals are highly ordered solid materials that form a lattice that extend to all directions. The smallest repeating group of particles is called the unit cell (Figure 4). The whole crystal can be thought consisting of repetitive copies of the unit cell along its principal axes. The lengths of unit cell edges and the angles between them are together called the lattice constants. The lattice constants define primitive lattice vectors $\vec{a_1}, \vec{a_2}$ and $\vec{a_3}$ that span the lattice. A translation along any linear combination of primitive vectors results in a position that looks exactly the same as the starting position.

Periodicity of crystals makes them easier to simulate compared to amorphous materials, since each unit cell in a perfect crystal is identical. That means that if wave function can be solved inside the unit cell, it is also known everywhere. That allows applying periodic boundary conditions when solving wave function of a crystal by requiring that the wave function must have the same periodicity as the crystal.

Periodic boundary conditions in a crystal lead to Bloch wave. If translation $\hat{T}$ is a linear combination of primitive lattice vectors $\vec{a_1}, \vec{a_2}$ and $\vec{a_3}$, ie. the crystal is periodic for translation $\hat{T}$, the translation will add a phase factor to the wave function:

$$\psi_a\left(\vec{k}, \vec{r}\right) = \exp\left(i\vec{k} \cdot \vec{r}\right) u_a\left(\vec{k}, \vec{r}\right), \tag{56}$$

where u_a is a function with the same periodity as the crystal.

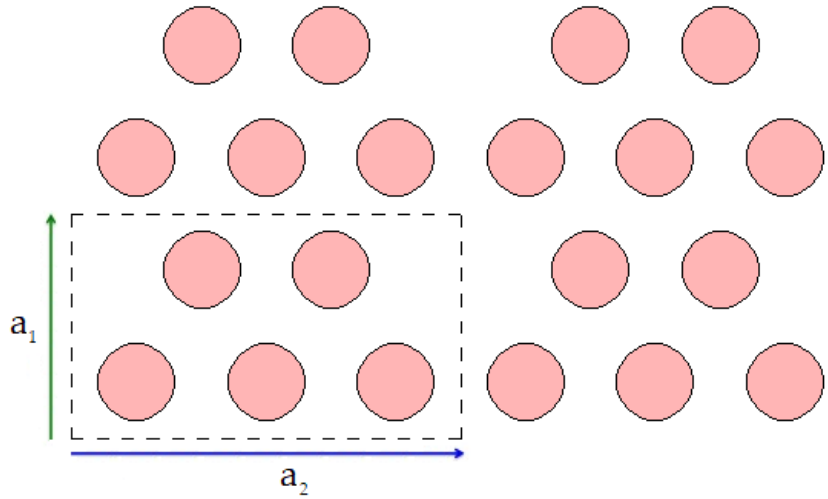

Figure 4. Unit cell (rectangle) of β_{12} borophene and primitive vectors $\vec{a_1}$ and $\vec{a_2}$.

According to Bloch's theorem, electrons in perfect crystal have a basis of Bloch waves, each of which is an energy eigenstate. This means that instead of using a basis of localized atomic orbitals, Bloch waves can be used as a basis instead for periodic crystals. Thus basis functions φ_μ become [19]

$$\varphi_\mu\left(\vec{k},\vec{r}\right) = \frac{1}{\sqrt{N}}\sum_{\vec{T}} \exp\left(i\vec{k}\cdot\vec{T}\right)\varphi_\mu\left(\vec{r}-\vec{T}\right), \tag{57}$$

where N is the number of unit cells in the crystal, technically infinite in this case.

Koskinen and Kit present a formalism to generalize Bloch's theorem further in their paper [21]. Koskinen and Kit show in their paper that if potential for which electrons are exposed is invariant for a symmetry operation $\hat{S}$, the wavefunction of the structure picks up a phase factor. This is essentially just revised Bloch's theorem.

Revised periodic boundary conditions are interesting from viewpoint of atomic simulations, since they allow simulating twisted or bent structures. Bending can be approximated with translations and rotations of the unit cell (Figure 5) as long as the bending curvature R is sufficiently large compared to the size of the unit cell. Revised periodic boundary conditions offer a method to easily compute the effects of these translations and rotations on orbitals, and thus it is an effective method for simulation of bending.

To model bending, symmetry operations $\hat{S}$ consisting of translations and rotations are required. For the purposes of this study, the interest is in symmetry operations $\hat{S}_i\left(\theta_i, \Delta z_i\right)$ that involve only rotation around z-axis and translations within z-axis:

$$\hat{S}_i\left(\theta_i, \Delta z_i\right) = \hat{R}_z\left(\theta_i\right)\hat{T}_z\left(\Delta z_i\right). \tag{58}$$

Constructing a bent sheet requires two symmetry operations $\hat{S}_1$ and $\hat{S}_2$ (Figure 5). For rectangular unit cell that is aligned within z-axis, symmetry operations are

$$\hat{S}_1 = \hat{R}_z\left(\frac{-b\sin\left(\phi\right)}{R}\right)\hat{T}_z\left(b\cos\left(\phi\right)\right) \tag{59}$$

$$\hat{S}_2 = \hat{R}_z\left(\frac{a\cos\left(\phi\right)}{R}\right)\hat{T}_z\left(a\sin\left(\phi\right)\right), \tag{60}$$

where a and b are unit cell constants, R is bending curvature and ϕ is the rotation angle of unit cell around its normal vector (lattice angle, Figure 6).

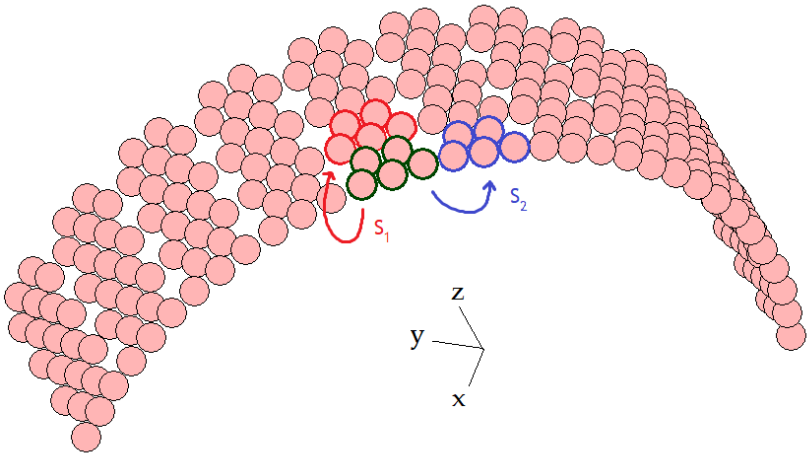

Figure 5. Effects of symmetry operations $\hat{S}_1$ and $\hat{S}_2$. Operation $\hat{S}_1$ corresponds to translation of 1.62 Å and rotation of 0° (red) and operation $\hat{S}_2$ translation of 2.87 Å and rotation of 8.2° (blue). Bending curvature $R = 20$ Å and lattice angle $\phi = 0°$. The sheet is effectively bending around the z-axis.

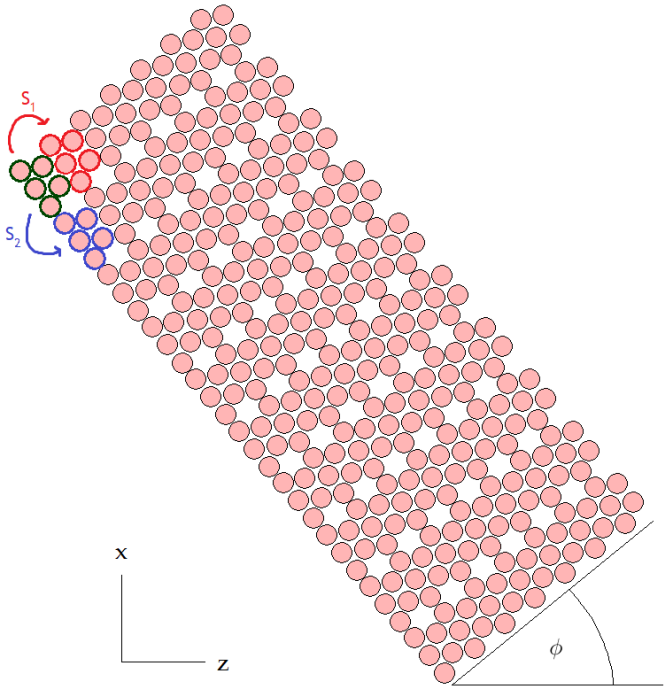

Figure 6. Illustration of lattice angle $\phi = 40°$ from xz-plane. Bending curvature is large ($R = 200$ Å) so the structure appears planar. Decreasing bending curvature would result in the sheet bending more clearly around the z-axis.

3 Parametrization

This section describes parametrization process, which is a significant part of the whole study. The purpose of parametrization is to obtain parameters required for computation of pseudo-atom orbitals and approximate mathematically complicated repulsive energy term E_{rep}. Orbital energies ϵ_{2s} and ϵ_{2p}, FWHM of density fluctuations and Hubbard U are parameters that are directly obtained with DFT while pseudo-atom confinement factor x and orbital cut-off radius R_{cut} are obtained by manual iteration. The repulsive energy term is obtained by fitting derivative of repulsion for boron-boron bonds in different structures and computing energy curve from the derivative. Energies and bond lengths of these structures can be obtained from DFT-calculations but they can also simply be taken from experimental results. Parametrization has to be done individually for each element pair that have bonds with each other in the studied material.

Band structure is responsible for majority of contribution to total energy, and thus without correct band structure it is impossible to get other properties right either [19]. That is why during parametrization band structure is the first thing considered. Since this study ultimately aims to model bending of borophene sheets, elastic constants are also used in benchmarking. Elastic constants can be obtained simply from stretching sheets and making quadratic fit on energy curve.

Calculations are performed with Hotbit, which is an python-based open source DFTB calculator that is designed for Atomic Simulation Environment (ASE). Most steps of parametrization can be done with scripts readily available in Hotbit, such as computing Slater-Koster tables and fitting the repulsive potential. Certain DFT-calculations are required in parametrization but they are performed only once and are saved into lookup tables.

3.1 Repulsive energy term

In theoretic background it was concluded that repulsive energy term can be approximated as

$$E_{\text{rep}} = \sum_{I<J} V_{\text{rep}}^{IJ}\left(R_{IJ}\right). \tag{61}$$

The problem is now constructing an approximate repulsive potential E_{rep}. The general idea is finding a function for repulsive potential that, together with other parameters, can approximately reproduce known properties. Repulsive potential is assumed to be smooth and monotonic so that it is transferable for actual structures of interest.

However in practice repulsive potential is not constructed directly. Instead it is obtained from minimizing force differences $\left|\vec{F}^{\text{DFT}} - \vec{F}^{\text{DFTB}}\right|$ for reference structures and thus finding derivative of repulsive potential.

For a homonuclear system (such as borophene) total force on atom I with DFTB can be written is form

$$\vec{F}_I = \vec{F}_I^0 + \sum_{J\neq I} V'_{\text{rep}}\left(R_{IJ}\right)\vec{R}_{IJ} \tag{62}$$

$$= \vec{F}_I^0 + \sum_{J\neq I} \epsilon_{IJ}\vec{R}_{IJ}, \tag{63}$$

where $\vec{F}_I^0$ contains all other forces than repulsion and can thus be evaluated as it is.

Data from reference structures form a set of points $\{ R_i, V'_{\text{rep},i} \}$ which can be used to minimize the sum $\sum_I \left|\vec{F}_I^{\text{DFT}} - \vec{F}_I\right|$. The function applied for repulsive potential in Hotbit is smoothing spline, which yields a functional minimization problem

$$S\left[V'_{\text{rep}}\left(R\right)\right] = \sum_{i=1}^{M}\left(\frac{V'_{\text{rep},i} - V'_{\text{rep}}\left(R_i\right)}{\sigma_i}\right)^2 + s\int^{R_{\text{cut}}} V'''_{\text{rep}}\left(R_i\right)^2 dR, \tag{64}$$

where s is parameter controlling smoothness and σ_i are weights of points. The weights σ_i are tunable parameters that can be used to alter relative weights of different structures at different bond length, for example to have larger weight for dimer curve at small distances. R_{cut} is a parameter that determines the distance where repulsion becomes 0. It is an essential parameter since it must be small enough to only contain the directly neighbouring atoms.

Repulsive potential $V_{\text{rep}}\left(R\right)$ is then obtained from its derivative

$$V_{\text{rep}}\left(R\right) = -\int_R^{R_{\text{cut}}} V'_{\text{rep}}\left(r\right) dr. \tag{65}$$

3.2 Parametrization process and benchmarking

The purpose of benchmarking is to compare properties computed with DFTB to known results, adjust parameters and evaluate whether the parametrization is capable of producing reliable results. Initially most important property is to get band structure that appears correct, since band structure energy has the largest contribution to total energy. Only after DFTB band structure resembles that of DFT remaining parameters can be optimized.

The most important parameter affecting band structure is pseudo-atom confinement r_0. Typically used starting point for r_0 is twice the covalent radius of the dimer. Usually it is the only parameter affecting band structure that has to be considered in parametrization, although if initially obtained band structure appears unrealistic, other parameters such as orbital energies have to be modified.

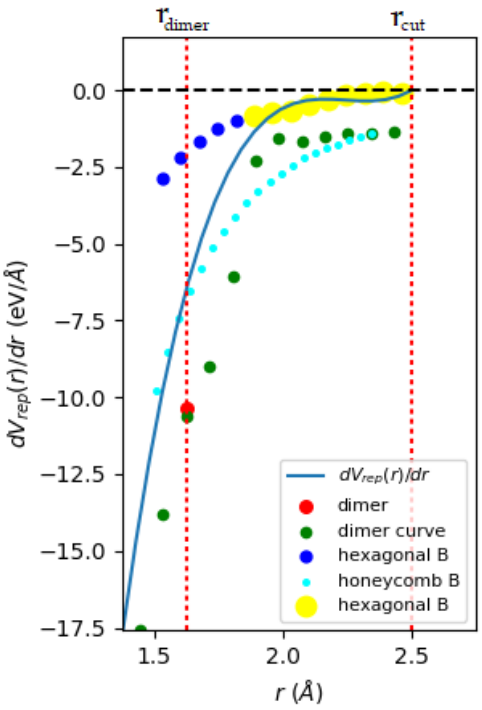

Figure 7. Fitted derivative of repulsion dV_{rep}/dr. Data points: Computed dimer equilibrium point (red), full dimer curve (green), hexagonal borophene (blue and yellow), and honeycomb borophene (cyan). Size of the circle corresponds relative weight of the data point. Curve of hexagonal borophene was cut into to parts to reduce weight of the curve at short distances, since it differed from rest of the points, causing instable structures.

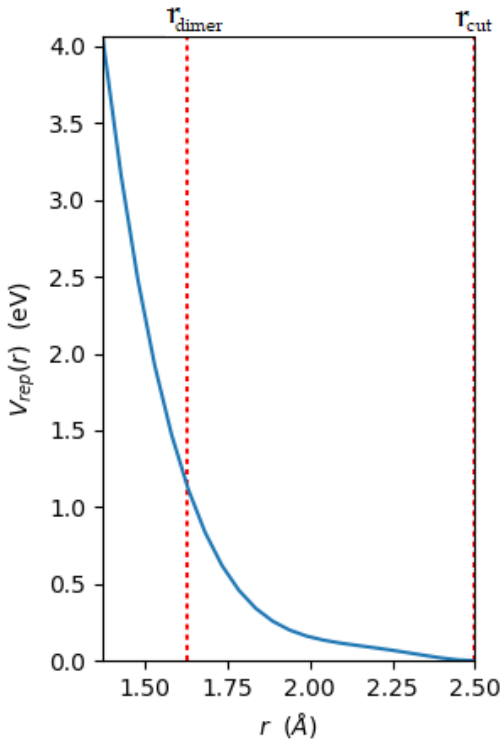

Figure 8. Repulsive potential V_{rep} obtained from its derivative (Figure 7).

Fitting the repulsive potential is less straightforward. There are multiple variables affecting the fit: pseudo-atom confinement factor x, cut-off radius R_{cut}, and weights σ_i given for points in fitting. Finding suitable weights may be problematic, since point sets of different structures are sometimes scattered (Figure 7). The general idea is to choose such values for x and R_{cut} so that the point set appears aligned on the fitted curve.

There is no automatic process for full parametrization. In practice the parametrization procedure consists of numerous rounds of small changes to parameters and computing properties used in benchmarking and repeating the procedure. It should be noted that parameters with physical meaning cannot be chosen arbitrarily - if optimization produces physically unrealistic values, the issue is most likely in approximations made in the theory of DFTB.

In this work band structure, unit cell and elastic constants were considered in benchmarking. Fitted derivative of repulsive potential is presented in figure 7, the repulsion in figure 8 and parameters in table 1. The final set of parameters and computed benchmarking properties is a compromise. Lattice constants different from DFT results only slighly, but Young's moduli had a more significant error. No

Table 1. Final values of parameters.

Parameter	
ϵ_{2s}	-0.345 eV
ϵ_{2p}	-0.137 eV
FWHM	4.101 eV^{-1}
U	0.324 eV
r_{cov}	1.80 Å
x	1.4 Å
R_{cut}	2.5 Å

combination of parameters within physical range was found to correct the error. Poisson's ratios were even further from DFT results. In pro gradu of Johannes Nokelainen [22] there have been similar issues. In his pro gradu he computed Poisson's ratio of boron nitride monolayers with DFTB and the difference between DFTB and DFT results was approximately 150 % - an error of the same magnitude as here. That indicates that the source of error is most likely in approximations made in DFTB and that boron may be a difficult element to simulate with DFTB.

Certain notes should be made about the fit. Curves of different borophene structures do not align well into a line, which makes fitting more difficult and increases potential error. Since lengths of bonds in β_{12} and χ_3 sheets in this study fall mostly into range $r = 1.6 - 1.8$ Å, that is the most important area in fitting. At that particular range data points are unfortunately scattered, and that forced to search for optimal fit by trial-and-error by repeatedly computing properties used for benchmarking (Table 2) and also adjusting parameters to find the combination of parameters that leads to most consistent grouping of data points. In benchmarking weighing tail of data point of hexagonal borophene lattice yielded the most consistent results, although the same could also have been achieved by lowering R_{cut} (Figure 7).

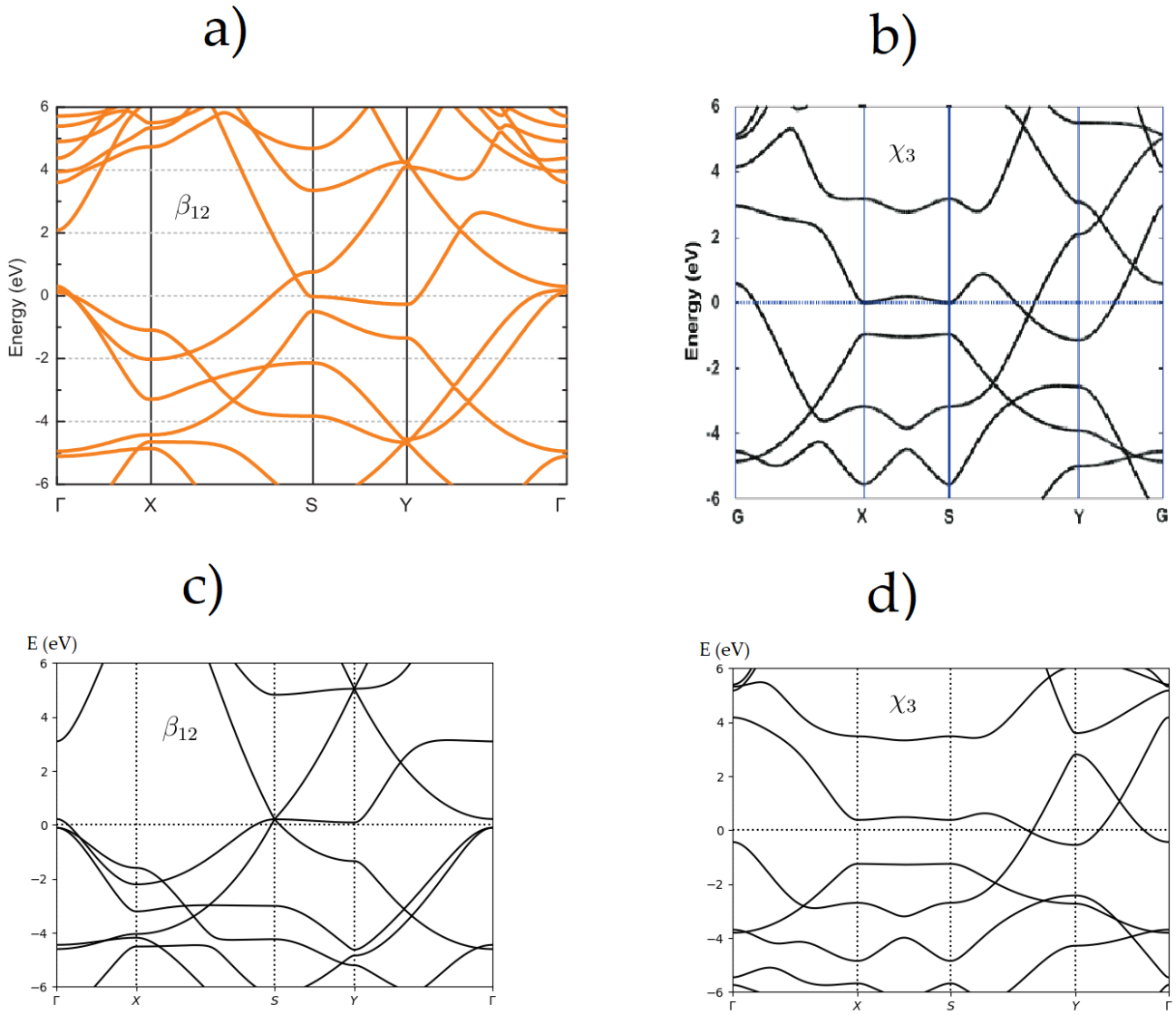

Figure 9. Band energies of β_{12} and χ_3 borophenes. a) β_{12} adapted with permission from Peng et al. [23], edited. Copyright 2017 the authors. b) χ_3 adapted with permission from by Vishkayi et al. [24], edited. Copyright 2018 PCCP. c-d) Their band energy with DFTB (this work).

Table 2. Computed unit cell, Young's modulus C and Poisson's ratio ν. Angle θ is the angle between principal lattice vectors in χ_3, which does not have rectangular unit cell. DFTB results are this work and those of DFT are from references [14] [23] used for benchmarking.

	a (Å)	b (Å)	C_x (N/m)	C_y (N/m)	ν_x	ν_y
β_{12} (DFTB)	5.09	2.93	172	199	0.44	0.40
β_{12} (DFT) [14] [23]	5.07	2.93	189	210	0.15	0.17
χ_3 (DFTB)	4.45	4.45	127	131	0.38	0.37
χ_3 (DFT) [14] [23]	4.45	4.45	196	208	0.11	0.12

4 Bending simulations

Simulation of bending is relatively easy with Hotbit, since it offers methods that make use of revised periodic boundary conditions. When a copy of the unit cell is translated and twisted appropriately and the process is repeated, it effectively creates a bent sheet. With revised periodic boundary conditions implemented, only one unit cell has to be considered in the simulation, which makes relaxation calculations relatively light. Thus the method is for simulating bent structures.

Obtaining bending modulus from simulations is simple. During bending, energy density follows relation $E_b = \kappa/(2r^2)$, where κ is bending stiffness and r is bending curvature. Bending stiffnesses of different borophene nanotubes have previously been computed for principal lattice directions with DFT, for example by Zhang et al. [14] Thus by varying bending curvature it is possible to obtain κ for that specific lattice angle (Figure 10), curvature radii $R = 30$ Å in each case. By repeating this process for varying lattice angle ϕ one then gets bending stiffness as a function of lattice angle, which is the goal of this study.

4.1 Bending stiffness

Results are presented in figure 11. The χ_3 sheet showed a clear minimum at $\phi = 40°$ with $\kappa = 0.45$ eV which quickly transitioned into a maximum of $\kappa = 0.95$ eV at $\phi = 80°$. This indicates that bending stiffness is highly dependent on lattice direction. However bending stiffness curve of β_{12} sheet raised more questions. Bending stiffness of β_{12} sheet was negative for various angles but it also had a region of positive bending stiffness between lattice directions 20° to 70°. Such a result is either spectacular or there's something wrong in the computation, so this demanded more investigation.

To determine whether DFTB result of negative bending stiffness was consistent, nanoribbons were simulated (Figure 12). Unlike infinite sheets, nanoribbons may form curvatures freely when the structure is relaxed. Thus when a bent nanoribbon is simulated, it should either stay non-planar or relax into planar configuration, depending on whether bending stiffness is negative or positive. This allows testing

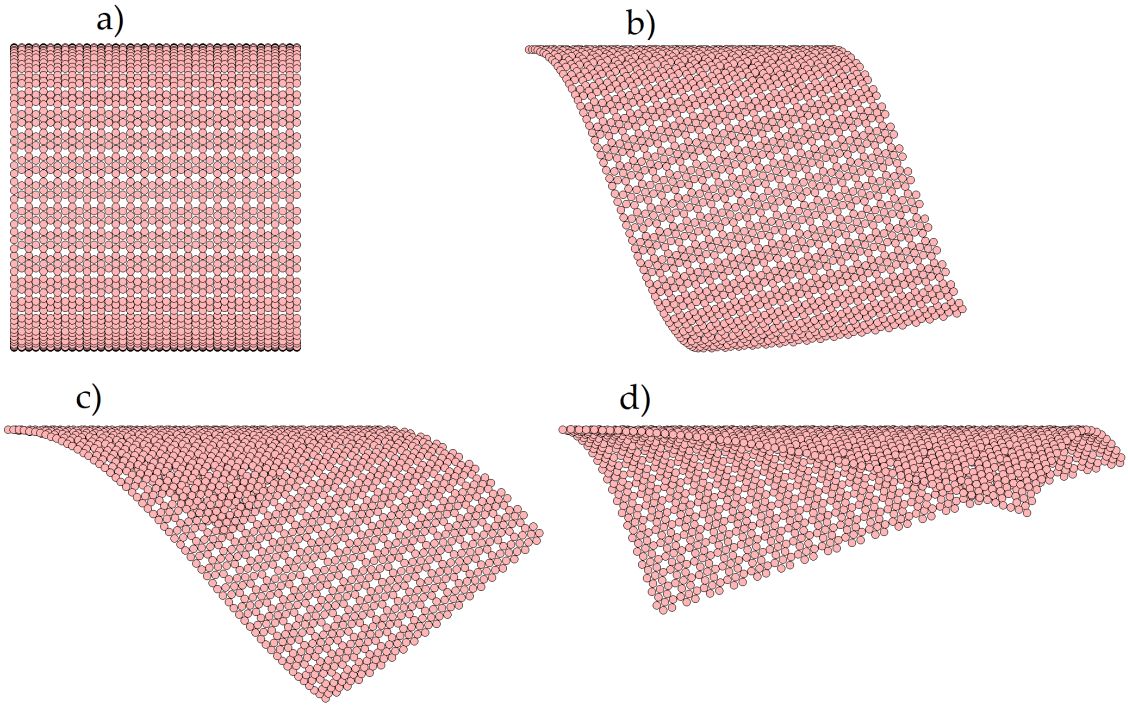

Figure 10. β_{12} lattices with bending curvature $R = 30$ Å. Lattice angle ϕ is a) 0°, b) 20°, c) 40° and d) 70°.

whether β_{12} lattice does prefer non-planar configuration, which would confirm consistency of negative bending stiffness of β_{12}. For comparison, χ_3 nanoribbons were simulated as well - they should behave the opposite way and settle to planar shape during relaxation.

The nanoribbons with different initial curvatures were then relaxed. As can be seen in figure 12, β_{12} nanoribbons indeed did start to form multi-centered curvatures. This indicates that result of negative bending stiffness is consistent. The χ_3 nanoribbons used as reference also behaved as expected: they relaxed into planar configurations.

As DFTB calculations were self-consistent, they were compared with DFT nanoribbon calculations. Since DFT optimization for bent borophene sheet failed to converge, optimization was also run for planar sheet. The DFT results were clear. DFT energy of β_{12} nanoribbons is lower in planar configuration than in bent configuration, which is conflicting with DFTB results. This unfortunately means that DFTB most likely has a fundamental flaw when it comes to boron structures, which makes DFTB calculations unreliable in that case.

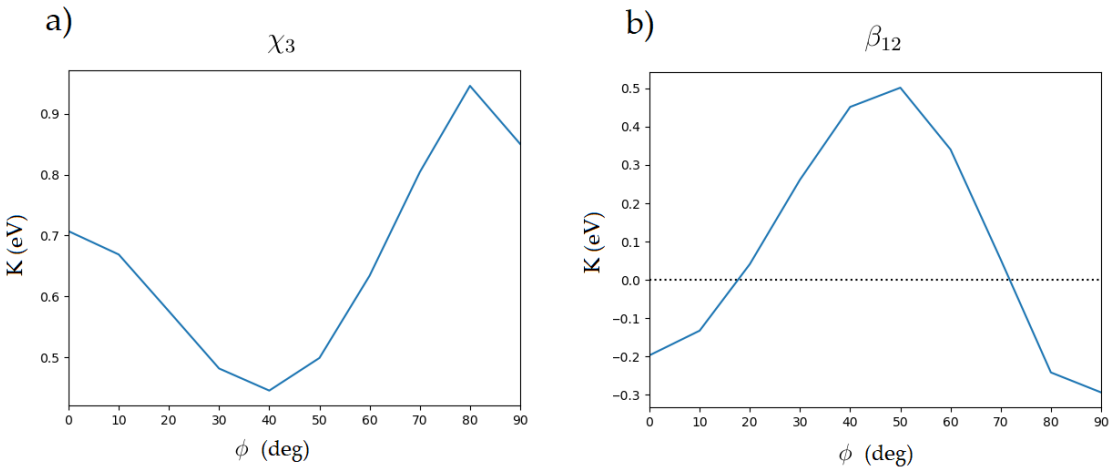

Figure 11. Bending stiffness as a function of the lattice angle. a) χ_3, b) β_{12}.

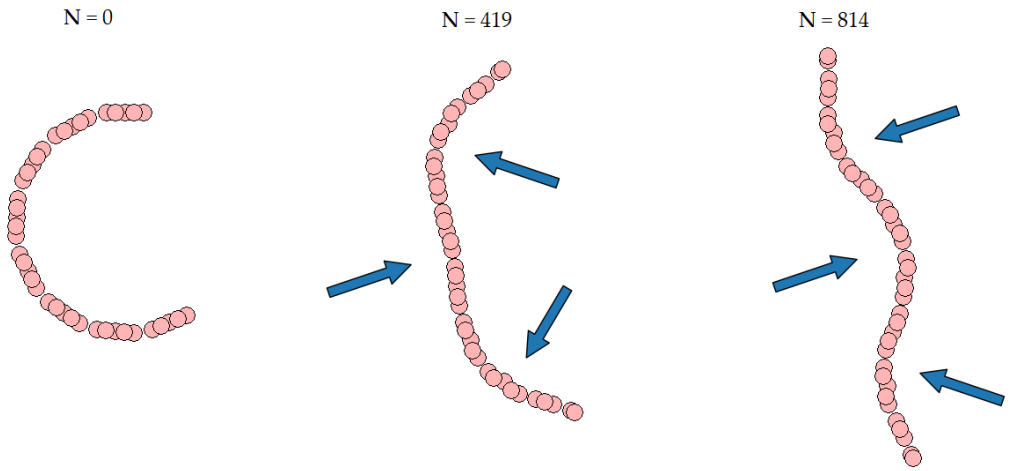

Figure 12. Simulation of bent β_{12} nanoribbon with DFTB. N is the number of optimization steps run. Initial configuration (left) is strongly bent with one center of curvature. Further in optimization (middle) three smaller curvatures start to form, marked with arrows. In the optimization result (right) the centers of curvature are clearly visible.

5 Conclusions

This study aimed to obtain bending stiffness as a function of lattice angle for two different types of borophene lattices, β_{12} and χ_3. While the computations did yield the desired curve, the results were exotic. DFTB predicted that certain lattice angles for β_{12} lattice were unstable and the sheet would rather form wave-like patterns. Comparison with DFT calculations for the same borophene lattices showed that the results of DFTB calculations are most likely inaccurate. That result is in agreement with problems that already rose during benchmarking, where DFTB was unable to replicate certain mechanical constants. Especially value of Poisson's ratio differed drastically between DFT and DFTB, an issue that has been seen before in DFTB calculations of boron-based structures [22].

It was nevertheless shown that DFTB is a useful method for quick structural analysis but that it also comes with significant downsides that have to be considered. Since DFTB is not an ab initio method but it rather relies on the assumption of tight-binding, there are cases when the approximations made are too crude. It is possible that boron's electron-deficit natures plays a role invalidating assumptions made in tight-binding, since the bonds between boron atoms differ from ideal covalent bonds. What approximations made in DFTB that cause problems in modeling boron is something that could be researched in the future by investigating different kind of boron compounds.

To conclude, while this study failed to illustrate capability of DFTB, it is still just as important to show what it is not capable of doing. All methods do have their weaknesses and one has to be aware of them. This is why lighter and more expensive computational methods both have their places. Sometimes the lighter method is applicable and thus preferrable, but when this is not the case, more accurate methods are required.

References

[1] K. S. Novoselov *et al.*, "Electric field effect in atomically thin carbon films", *Science*, vol. 306, no. 5696, pp. 666–669, 2004, ISSN: 0036-8075. DOI: 10.1126/science.1102896.

[2] M. Ashton *et al.*, "Topology-scaling identification of layered solids and stable exfoliated 2d materials", *Phys. Rev. Lett.*, vol. 118, p. 106 101, 10 Mar. 2017. DOI: 10.1103/PhysRevLett.118.106101.

[3] X. Cai *et al.*, "Preparation of 2d material dispersions and their applications", *Chem. Soc. Rev.*, vol. 47, pp. 6224–6266, 16 2018. DOI: 10.1039/C8CS00254A.

[4] Z. Zhang *et al.*, "Two-dimensional boron monolayers mediated by metal substrates", *Angewandte Chemie International Edition*, vol. 54, no. 44, pp. 13 022–13 026, 2015. DOI: 10.1002/anie.201505425.

[5] H. Tang and S. Ismail-Beigi, "Novel precursors for boron nanotubes: The competition of two-center and three-center bonding in boron sheets", *Phys. Rev. Lett.*, vol. 99, p. 115 501, 11 Sep. 2007. DOI: 10.1103/PhysRevLett.99.115501.

[6] S. Er, G. A. de Wijs, and G. Brocks, "Dft study of planar boron sheets: A new template for hydrogen storage", *The Journal of Physical Chemistry C*, vol. 113, no. 43, pp. 18 962–18 967, 2009. DOI: 10.1021/jp9077079.

[7] C. Zhang *et al.*, "Li adsorption on monolayer and bilayer MoS2 as an ideal substrate for hydrogen storage", *Chinese Physics B*, vol. 27, no. 6, p. 066 103, Jun. 2018. DOI: 10.1088/1674-1056/27/6/066103.

[8] F. Li *et al.*, "First-principles study of hydrogen storage on li-decorated silicene", *Journal of Nanoparticle Research*, vol. 15, no. 10, p. 1972, Sep. 2013, ISSN: 1572-896X. DOI: 10.1007/s11051-013-1972-z.

[9] C. Ataca *et al.*, "High-capacity hydrogen storage by metallized graphene", *Applied Physics Letters*, vol. 93, no. 4, p. 043 123, 2008. DOI: 10.1063/1.2963976.

[10] X. Zhang *et al.*, "Borophene as an extremely high capacity electrode material for li-ion and na-ion batteries", *Nanoscale*, vol. 8, pp. 15 340–15 347, 33 2016. DOI: 10.1039/C6NR04186H.

[11] Z.-Q. Wang *et al.*, "Review of borophene and its potential applications", *Frontiers of Physics*, vol. 14, no. 3, p. 33 403, Apr. 2019, ISSN: 2095-0470. DOI: 10.1007/s11467-019-0884-5.

[12] A. J. Mannix *et al.*, "Synthesis of borophenes: Anisotropic, two-dimensional boron polymorphs", *Science*, vol. 350, pp. 1513–1516, 6267 Dec. 2015. DOI: doi:10.1126/science.aad1080.

[13] A. K. Singh, A. Sadrzadeh, and B. I. Yakobson, "Probing properties of boron α-tubes by ab initio calculations", *Nano Letters*, vol. 8, no. 5, pp. 1314–1317, 2008, PMID: 18376872. DOI: 10.1021/nl073295o.

[14] Z. Zhang *et al.*, "Elasticity, flexibility, and ideal strength of borophenes", *Advanced Functional Materials*, vol. 27, no. 9, p. 1 605 059, Jan. 2017, ISSN: 1616-301X. DOI: 10.1002/adfm.201605059.

[15] P. Hohenberg and W. Kohn, "Inhomogeneous electron gas", *Phys. Rev.*, vol. 136, B864–B871, 3B Nov. 1964. DOI: 10.1103/PhysRev.136.B864.

[16] W. Kohn and L. J. Sham, "Self-consistent equations including exchange and correlation effects", *Phys. Rev.*, vol. 140, A1133–A1138, 4A Nov. 1965. DOI: 10.1103/PhysRev.140.A1133.

[17] W. M. C. Foulkes and R. Haydock, "Tight-binding models and density-functional theory", *Phys. Rev. B*, vol. 39, pp. 12 520–12 536, 17 Jun. 1989. DOI: 10.1103/PhysRevB.39.12520.

[18] O. O. Kit, L. Pastewka, and P. Koskinen, "Revised periodic boundary conditions: Fundamentals, electrostatics, and the tight-binding approximation", *Physical Review B*, vol. 84, no. 15, Oct. 2011, ISSN: 1550-235X. DOI: 10.1103/physrevb.84.155431.

[19] P. Koskinen and V. Mäkinen, "Density-functional tight-binding for beginners", *Computational Materials Science*, vol. 47, no. 1, pp. 237–253, 2009. DOI: https://doi.org/10.1016/j.commatsci.2009.07.013.

[20] M. Elstner *et al.*, "Self-consistent-charge density-functional tight-binding method for simulations of complex materials properties", *Phys. Rev. B*, vol. 58, pp. 7260–7268, 11 Sep. 1998. DOI: 10.1103/PhysRevB.58.7260.

[21] P. Koskinen and O. O. Kit, "Efficient approach for simulating distorted materials", *Phys. Rev. Lett.*, vol. 105, p. 106 401, 10 Aug. 2010. DOI: 10.1103/PhysRevLett.105.106401.

[22] J. Nokelainen, "Computational modelling of boron nitride nanostructures based on density-functional tight-binding", University of Jyväskylä, Master's thesis, 2014.

[23] B. Peng *et al.*, "Stability and strength of atomically thin borophene from first principles calculations", *Materials Research Letters*, vol. 5, no. 6, pp. 399–407, 2017. DOI: 10.1080/21663831.2017.1298539.

[24] S. Izadi Vishkayi and M. Bagheri Tagani, "Freestanding χ_3-borophene nanoribbons: A density functional theory investigation", *Phys. Chem. Chem. Phys.*, vol. 20, pp. 10 493–10 501, 15 2018. DOI: 10.1039/C7CP08671G.